journal

J. Am. Ceram. Soc., ■■ [■■] 1–9 (2011)
DOI: 10.1111/j.1551-2916.2011.04572.x

Dynamics of the Freezing Front During the Solidification of a Colloidal Alumina Aqueous Suspension: *In Situ* X-Ray Radiography, Tomography, and Modeling

Andrea Bareggi[†] and Eric Maire

Université de Lyon, INSA-Lyon, MATEIS CNRS UMR5510, F-69621 Villeurbanne, France

Audrey Lasalle and Sylvain Deville

Laboratory of Synthesis and Functionalization of Ceramics, UMR3080 CNRS/Saint-Gobain CREE, BP 20224, 84306 Cavaillon Cedex, France

Ice templating of colloidal suspension is gaining interest in material science because it offers the possibility to shape advanced materials, in particular porous ceramics. Recent investigations on this process show that a correlation between the morphology of the frozen suspension and the velocity of the freezing front do exist. The dynamics of the freezing front of a colloidal suspension of alumina is investigated in this study by experimental tests, finite element analysis, and analytical calculations. The experimental tests are carried out by *in situ* X-ray radiography (dynamics of the freezing front) and tomography (morphology of the frozen suspension). The finite element model is a continuous properties model; it is used for investigating the dynamics and the shape of the freezing front. The analytical model is based on the two-phase Stefan problem. We propose a solution for the dynamics of the solidification front based on the calculation of the diffusivity as a function of the particle fraction and local temperature.

Nomenclature

C_p	specific heat capacity of the suspension
D	diffusivity coefficient
D_0	Einstein–Stokes diffusivity
$h(t)$	solidification front position
Le	Lewis number
L_f	Latent heat of fusion of medium (water)
k_B	constant of Boltzmann
k_T	thermal conductivity of the suspension
R	radius of the alumina particle
St	Stefan number
T	local temperature
T_b	temperature at the base of the mold
$T_f(\phi)$	freezing temperature
T_m	melting temperature of the medium (water)
v_p	volume of the alumina particle
$z(\phi)$	dimensionless compressibility factor
α	thermal diffusivity of the suspension
η	similarity variable of the Stefan problem
θ	dimensionless temperature
θ_b	dimensionless temp. (base of the mold)
θ_f	freezing dimensionless temperature
θ_m	melting dimensionless temperature (water)
$\lambda(t)$	similarity variable at the interface
μ	viscosity of the medium (water)
ρ	density of the suspension
$\Pi(\Phi)$	osmotic pressure of the suspension
ϕ	particle fraction
ϕ_p	packing particle fraction
ϕ_{vol}	nominal volumetric particle fraction

I. Introduction

SINCE 1954, ice templating, also known as freeze casting, is an environmental friendly and cost-effective shaping process for advanced ceramic materials[1] with interconnecting pore channels or pore gradients in ceramic bodies.[2] Recent publications[3,4] show the wide range of application of ice templating. For introducing the pore structures in bulk ceramic bodies, suspensions with a low solid content are first frozen to obtain vehicle ice crystals that are often connected in dendritic shapes, surrounded by the frozen concentrated ceramic suspension.[2] After drying (removal of the ice by sublimation), porous channels remain, replicating the shape of the interconnected ice crystals. Ongoing research shows that the shape of the frozen structures and the porosity is particularly dependent on the speed of the freezing front.[5]

Sintered bodies of Al_2O_3 with aligned channels fabricated by unidirectional ice templating of aqueous ceramic slurries were reported.[6–8] These studies investigate the microstructure of the interconnected crystals of alumina, in relation to the velocity of the freezing front. The microstructure corresponding to the initial instants of solidification has been described in terms of crystal shape (R-crystals for the random structures, Z-crystals for the lamellar structures).[9] These investigations were carried out by high-resolution *in situ* X-ray radiography and tomography. The purpose of the present work is to investigate the kinetics of the freezing front of colloidal suspensions of alumina by X-ray radiography and tomography. The experimental observations are compared with the results obtained with a thermal finite element model (FEM) of the system (mold and colloidal suspension) and to the solution of the system of ordinary differential equations (ODE) (two-phase Stefan problem).

II. Materials and Methods

(1) Experimental Setup

The experimental part of this study focuses on the use of two nondestructive imaging techniques, the high-resolution X-ray absorption radiography and tomography. The use of tomography in materials science is relatively new.[10] The reconstructed

T. Ohji—contributing editor

Manuscript No. 28841. Received November 9, 2010; approved March 18, 2011.
This work was financially supported by the National Research Agency (ANR), project NACRE in the nonthematic BLANC programme, reference BLAN07-2_192446.
[†]Author to whom correspondence should be addressed. e-mail: bareggia@tcd.ie

three-dimensional map from X-ray tomography gives an indirect image of the microstructure. X-ray tomography was performed in the present study at a voxel size of (3.62 μm).[3] A set of 900 projections was taken within 180°. The complete technical description of the tomograph used can be found in Buffiere *et al.*[11] To summarize, this tomograph is equipped with a tungsten transmission target to produce a small size X-ray source, operated at 116 kV and 50 μA without filtering in the present study. The detector is an amorphous silicon flat panel made of 1900×1500 square pixels of 127 μm in lateral size.

Slurries were prepared by mixing distilled water with a small amount (0.2 wt% of the suspension) of ammonium polymethacrylate anionic dispersant (Darvan C, R. T. Vanderbilt Co., Norwalk, CT) and 32 vol% of alumina powder (Ceralox SPA 0.5, Sasol, Tucson, AZ, $D_{50} = 0.3$ μm, SSA 8 m^2/g).

Freezing experiments were performed by pouring the suspensions into a polypropylene cylindrical mold, invisible to X-rays, placed at the tip of a copper cold finger inside a cryogenic cell (see Fig. 1, right hand side for a scheme of the setup). The copper finger is cooled at its bottom using liquid nitrogen. This finger is 6 cm long so that the sample can be placed close to the X-ray tube for the high-resolution tomography. The conduction along the copper rod induces a decrease of the temperature at the bottom of the colloidal suspension. The cryogenic cell is composed of a double-wall PMMA envelope that prevents condensation or frost to accumulate and perturb the X-ray measurement. The atmosphere of the chamber is not refrigerated so that the suspension is forced to freeze from the bottom. Freezing kinetics is controlled by a resistance heater placed at the bottom of the copper rod using the information of the temperature measured by a thermocouple at the tip of the copper rod, close to the point where the solution touches the copper. The left side of Fig. 1 shows a close up of the sample, and the arrows indicate the heat flux and the temperature at the base of the sample. These boundary conditions are used in the FEM. The experimental setup was equipped with a PID controller for setting different temperature profiles to the mold. The PID controller was connected to a PC for recording the temperature profile during the solidification process. Five different temperature profiles were used: constant, linear, and three parabolic profiles. Radiographies were acquired in order to record the evolution of the freezing front. The acquisition frequency in the radiography was 1.4 Hz; therefore, the time span between two images was 0.71 s. The spatial resolution of radiography was chosen to be 11 μm. At this resolution, the entire polypropylene mold (16 mm of height, 3 mm of internal diameter) was visible on the CCD screen. The microstructure obtained by freezing the colloidal suspension was investigated by tomography. In order to keep the full width of the sample inside the field of view of the detector, a resolution of 3.62 μm was used.

(2) FEM

Incremental thermomechanical finite element simulations with two-dimensional axial symmetrical geometry simulated the kinematics of the freezing front. Figure 1 (left hand side) shows a sketch of the FEM. The equations numerically solved are the conduction (Fourier's law) and the convection equations. A thermal conductivity was defined for each component of the system and $h = 20\ W \cdot (m^2 \cdot K)^{-1}$ was used to represent the heat transfer coefficient to air. In order to simulate the thermal behavior of the suspension, a continuous properties model was considered. Because the region of the continuous phase transition is small in the temperature/enthalpy density diagram, the model is a good approximation of the dynamics of substances with discontinuous phase transitions.[12] Because the experimental tests show a relatively small zone of coexistence of the liquid and solid phases (and a well-defined ice front), this approximation

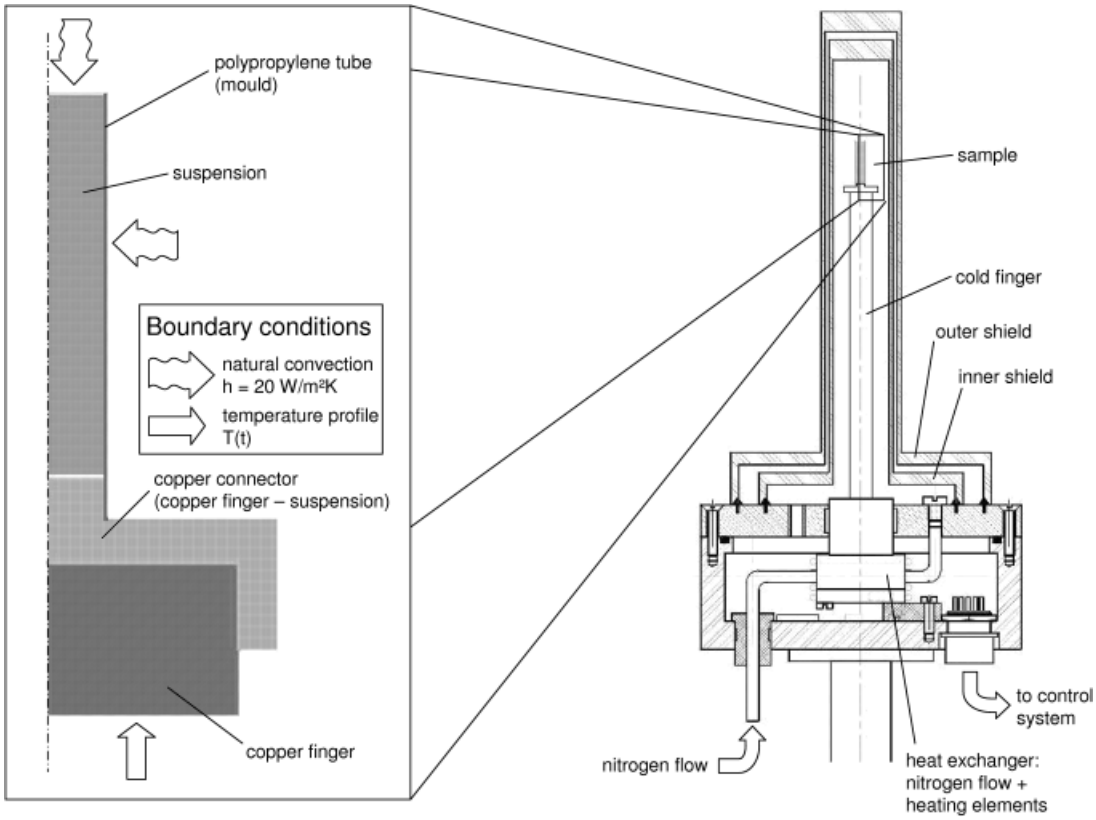

Fig. 1. Right: sketch of the freezing device. A flux of cold nitrogen is pumped at constant rate on a ring in contact with a copper finger, in contact with the colloidal suspension. A heating element controlled by a PID controller is used for regulating the temperature at the base of the suspension. A double shield provides thermal isolation from the ambient. Left: the geometry (cylindrical symmetry) and boundary conditions of the finite element model. The natural convection was applied to the upper boundary of the suspension and on the polypropylene mold.

is suitable for describing the overall thermodynamic behavior. In general, the thermal properties depend on local particle concentration. The results from X-ray tomography (Fig. 3) show the relative fraction of the concentrated particle zone (black zones), in comparison with the pure ice (white zones). The particle concentration is limited between the nominal volumetric concentration ($\phi_{vol} = 0.32$) and the maximum concentration ($\phi_p = 0.58$ is the breakthrough concentration), and between these limits the variation of the suspension properties due to the particle-rich phase fraction is relatively small. According to Peppin *et al.*,[13] the diffusivity and the freezing temperature depend on the particle fraction, as shown in Section II*(3)*. By considering a mean value of the suspension properties as a function of the local particle concentration, it is possible to apply the continuous properties FEM. The material properties used in the modeling, i.e., the thermal conductivity $k_T\,(W\cdot(m\cdot K)^{-1})$, the specific heat capacity $C_p\,(J\cdot(kg\cdot K)^{-1})$, and the density $\rho(kg/m^3)$, are shown in Table I. The properties of the suspension were calculated according to the equations presented in Section II*(3)* and Appendix A, and the thermal conductivity was estimated by the model of Jeffrey.[14] The main limitation of the continuous property model consists in the inability of reproducing fluctuations effects. The continuous property model does not account the rapid dendritic freezing occurring in the system; only planar and parabolic freezing front are predicted. Also the Stefan model described in the next paragraph applies to slow planar freezing and not to the rapid dendritic freezing. Such effect can be included by particle-based simulation methods as shown by Barr and Luijten.[15]

(3) Analytical Modeling

The Stefan problem[16] is a two-phase moving boundary problem that allows the calculation of the temperature field and the position of the interface between two phases in a melting or freezing process. The purpose of the model is to calculate the dynamics of the freezing front depending on the temperature profiles imposed at the base of the suspension. The temperature profiles are polynomials of the sixth order and reproduce the profiles used in the experimental tests. The physical assumptions for the application of the Stefan problem are conduction only, constant latent heat of fusion L_f, fixed melting temperature T_m, the interface between the two phases has no thickness, surface tension and ice nucleation are not considered (uniform freezing only).

The Stefan problem requires the estimation of the numbers of Stefan (*St*) and Lewis (*Le*) by using the dimensionless compressibility factor z as a function of particle fraction, which accounts for particle–particle interactions. The literature shows several attempts of estimating $z(\phi)$.[17–21] An approximation proposed by Peppin *et al.*[13] is valid over the entire concentration range, merges the results obtained by Woodcock[21] for concentration up to packing concentration, and the results by Carnahan and Starling[22] for low concentration (Fig. 2, upper side). The freezing temperature is also obtained as a function of the particle fraction (Fig. 2, lower side). The properties of the solution, such as the heat capacity and the density, depend on the particle fraction, as shown by Fig. 3 (upper side). The estimated *St* and *Le* numbers are plotted in Fig. 3 (lower side) as a function of the particle fraction, and the diffusivity coefficient D is plotted in Fig. 4 as a function of the temperature of the suspension and the particle fraction. The number of Lewis indicates the influence of the Brownian diffusion on the motion of particles. At relatively small particle radius (0.5–1 μm), a Lewis number $Le = 230$–250 is expected.[23,24] At this value, the velocity of the freezing front is small, compared with the particles velocity due to Brownian diffusion, high for small particles. Peppin observed that at small Lewis number, the concentration and the temperature profiles resemble those observed during alloy solidification, while for high Lewis number the weak or absent Brownian diffusion allows the formation of a porous medium ahead of the freezing front and the possibility of a morphological instability. In certain cases, the interface can become unstable owing to supercooling and particle engulfment at high front velocity.[25] If such instability is present during the solidification of a colloidal suspension, a variation in the freezing front velocity $\frac{\partial h}{\partial t}$ and a variation in the quantity $\phi\lambda$ are induced, with a consequent acceleration (or deceleration) of the front and a discontinuity in the particle fraction.

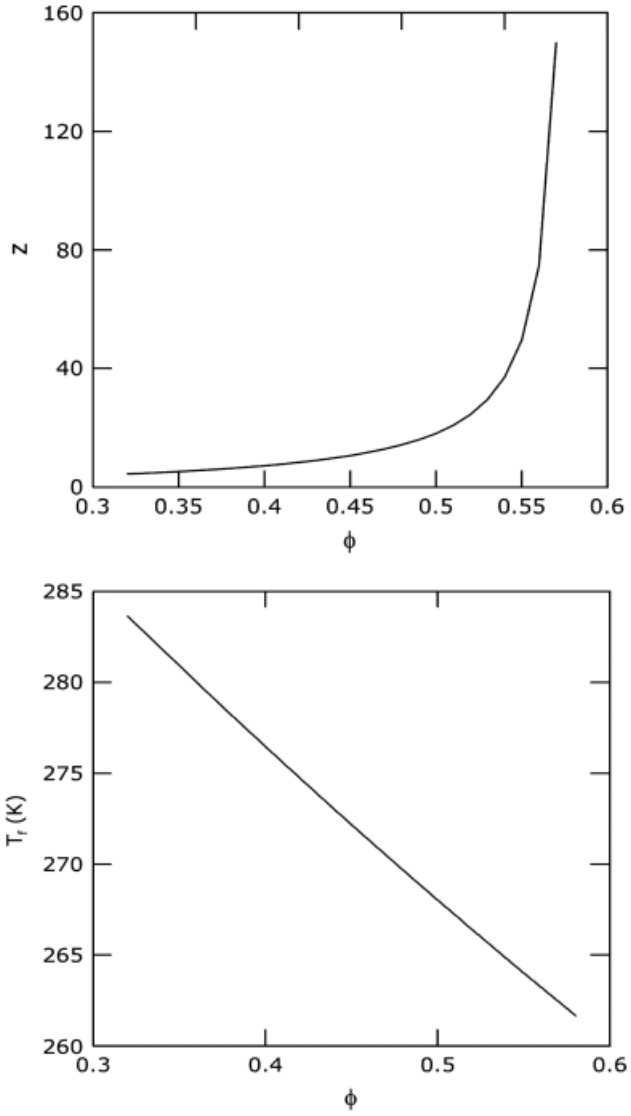

Fig. 2. The dimensionless compressibility factor z (upper side), the freezing temperature T_f expressed in K (lower side) as a function on the particle fraction Φ.

Table I. Thermal Properties (FEM and Analytical Modeling)

	L-phase	S-phase	Copper	Polypropylene
$k_T\,(W\cdot(m\cdot K)^{-1})$	0.6	0.9187	403	0.12
$C_p\,(J\cdot(kg\cdot K)^{-1}$	2434	1457	385	1925
$\rho\,(kg/m^3)$	2426	2218	8930	950

III. Results and Discussion

The results of experimental tests consist in morphological observation and quantitative information on the dynamics of the solidification process. The morphology was experimentally investigated by X-ray tomography, and the results about

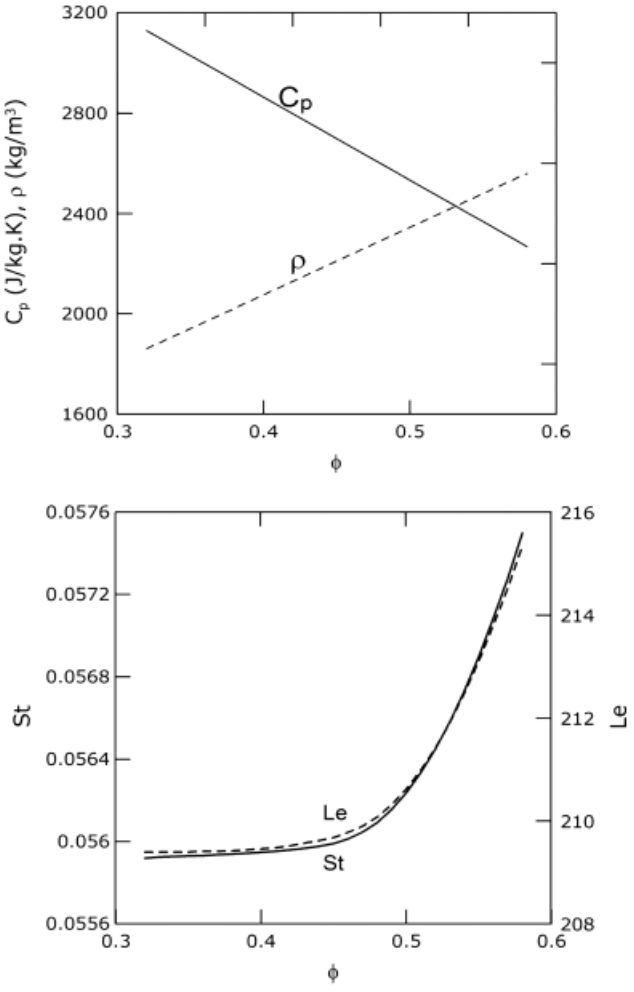

Fig. 3. The specific heat capacity C_p and the density ρ for the liquid phase of the suspension (upper side). The Stefan and Lewis used in the Stefan problem (lower side) as a function on the particle fraction Φ.

dynamics, obtained by radiography, was compared with the results obtained by FEM and to the solution of the Stefan problem obtained by numerical solved ODE.

(1) Morphology

Four zones can be morphologically distinguished in the frozen suspension.[9] Figure 5 shows a sample of the frozen suspension and the four zone qualitatively identified by the morphology of the crystals (on the left) and the corresponding slices obtained by X-ray tomography (black and white, on the right). In these images, the white part represents the ice, and the black part represents the alumina particle-rich regions. Morphologically speaking, the crystals can be classified into "R-crystals" (random symmetry, rejecting the alumina particles in *z*-direction) and "Z-crystals" (vertically aligned with the axis of the mold, rejecting the particles in the *x*- and *y*-directions). The goal of a directional ice templating technique is to obtain a structure mainly composed of Z-crystals. According to the qualitative observation,[9] only the last zone of the sample (*D*) is purely composed of Z-crystals. Table II shows the morphological zone in the frozen alumina suspensions.

In the zone between 0 and 3 mm of distance from the base of the mold, the resolution of the tomography was not able to show the crystals and particles distribution, therefore the microstructure is unknown. However, the freezing front is detectable and the measured interface velocity is particularly high (approximately 0.5–1 mm/s).

The Zone A starts as the resolution of the tomograph (voxel size: 3.62^3 μm^3) allows to obtain quantitative information on the size of the crystals. This zone is characterized by a rapid growth of the R-crystals. The velocity of the freezing front is diminishing to approximately 0.15 mm/s.

The Zone B corresponds to the transition between the zone A, populated by R-crystals only, and the region that shows both R-crystals and Z-crystals (zone C).

In the zone C, the entrapped particles reach a local maximum corresponding to the packing fraction at this particular interface velocity. The thickness of this zone is strongly dependent on the temperature gradient and the cooling temperature profile. If the temperature gradient is not present (constant temperature), the zone C extends until the end of the solidification process.

The zone D represents a steady-state condition because it is composed mainly of Z-crystals that extend vertically until the end of the solidification process. Particles redistribution is occurring in the *xy* plane. The particle fraction is reducing almost linearly. The zone D presents thin vertical ice structures, separated by alumina-packed particles, interconnected by thin horizontal alumina structures. Morphologically speaking, it is the only stable zone in the ice templating technique.

Figure 6 shows the frozen samples obtained by using five different cooling profiles. The diagram shows the repartition of the morphological zone for each sample. The exact position of the zone B was identified by the measurement of the particle fraction, rather than using the visual analysis. The darkening corresponds to a rapid increase of the particle-rich phase fraction, followed by a morphological mutation of the crystals: the R-crystals stop growing and they are progressively replaced by Z-crystals. The positions and the extensions of the zone B are easily identified by the curves of the particle fraction as a function of distance from the copper cold surface (the zone comprised between the local minimum and maximum of the particle fraction), shown in the second diagram of Fig. 7, while the first diagram shows the temperature profiles as a function of time. In the diagram of the particle fraction, the curve *par3* is not represented because it shows extremely little difference compared with the curve *par1*. The extension of the zone B seems to be larger in the curves than in Fig. 6. In the case considered, the solidification front is a parabolic surface that presents a local maximum at the axis of the cylindrical mold. Because in Fig. 6 the intersection of the conical surface with the mold is visible, the zone B appears smaller than in the tomographic reconstructions. The particle-rich phase fraction at the beginning of zone A is approximately 0.57 for all the samples, and then it diminishes with different inclination to a local minimum. The behavior of the particle fraction obtained with the constant temperature profile is quite different from the others in terms of extension of the zone B (the distance between local minimum and maximum particle fraction in the transition zone) and particle fraction at the end of the solidification process. Because the transition zone is associated with the reduction of the population of R-crystals and the growth of the population of Z-crystals, a weak transition zone lead to an extended zone C, i.e. when the difference between the minimum and maximum particle fraction is relatively small (such as in the case of constant temperature profile). The sample with constant temperature profile does not show any zone with Z-crystals, because the velocity of the interface after the transition zone C is so low that the Z-crystals cannot grow. It should be noted that the value of the constant temperature profile is close to the theoretical freezing temperature calculated in Eq. (A-8). As the temperature profile approaches the freezing temperature, the transition zone became weaker. Out of this range, it is not possible to describe the morphology of the frozen suspension in terms of Z-crystals and R-crystals, as done for the linear and parabolic temperature profiles used in this paper. The minimum extension of the transition zone is obtained with parabolic profiles ("*par1*" in particular), while the zone D is maximized. A low temperature also tends to shift the transition zone backward to the cold finger, allowing more space for the steady-state zone D. Not surprisingly, the condition that max-

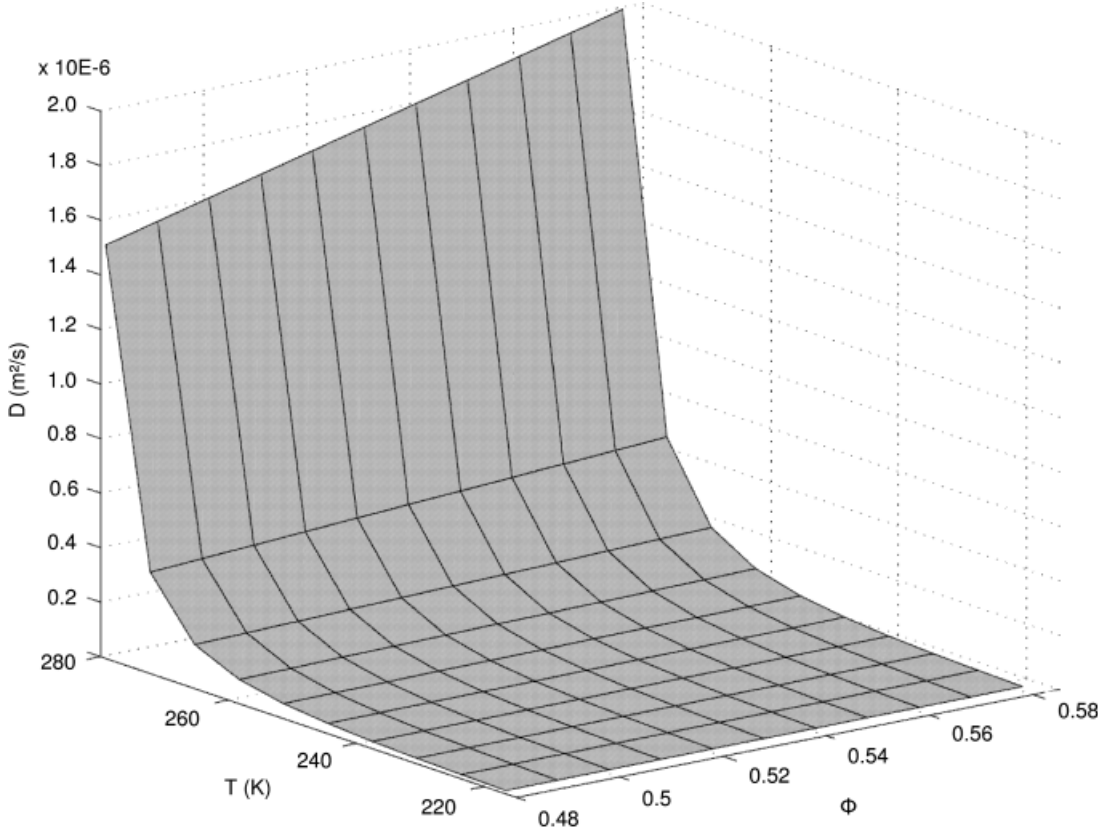

Fig. 4. The diffusivity coefficient D as a function of local temperature and particle fraction.

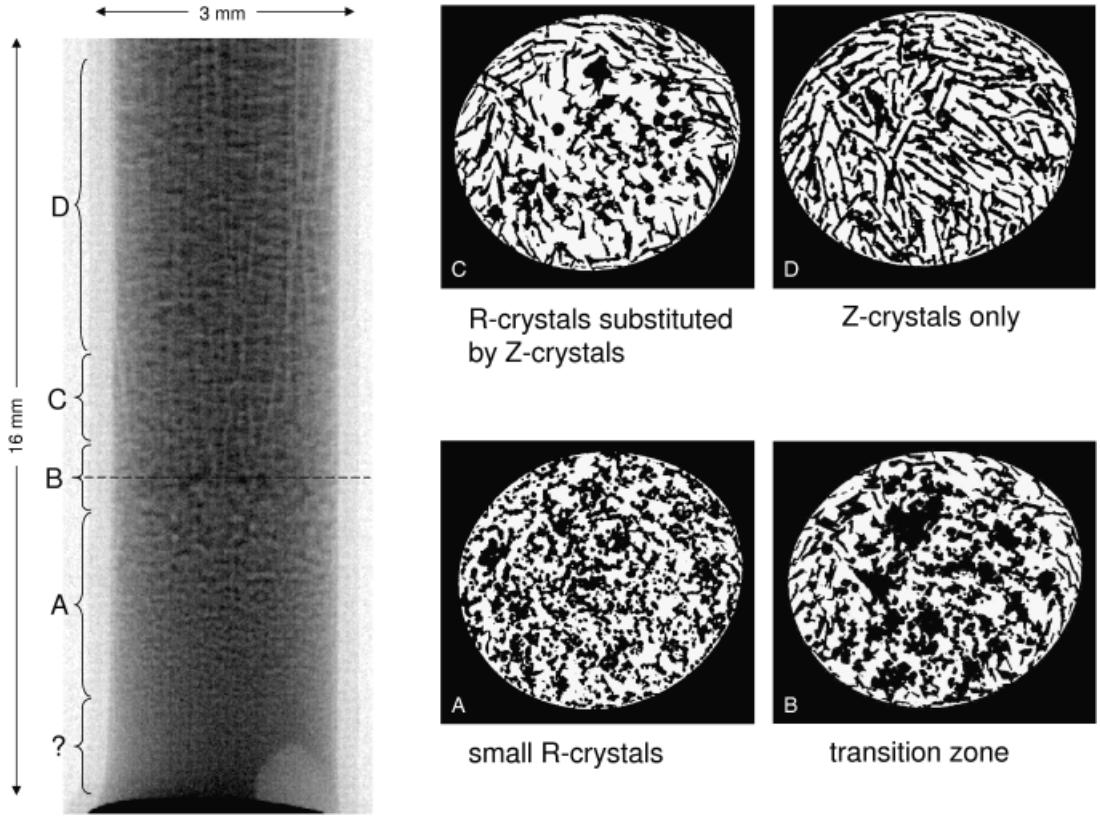

Fig. 5. The result of the radiography of the alumina sample frozen with the temperature profile "par1." The sample measures 16 mm in height and 3 mm in mean diameter. The morphological zones are indicated in the diagram on the left. The three slices on the right indicate the results of X-ray tomography. The bottom slice shows the suspension at the upper limit of zone A (small R-crystals). The middle slice shows the suspension in the zone B: R-crystals rapidly grow and few Z-crystals nucleate close to the polypropylene mold; because the zone C is approaching, the biggest R-crystals tent to group. The upper slice shows the suspension in the zone D (steady-state zone), characterized by Z-crystals.

Table II. Morphological Zones

Zone	R-crystals	Z-crystals	Morphological stability
A	Growing	Growing	No
B	Stop growth	Growing	No
C	No	Growing	No
D	No	Yes	Yes

imizes the zone D is a steep supercooled temperature profile, possibly parabolic.

(2) Dynamics

In the experimental tests, a systematic error is generated by the shape of the solidification front. In the initial phase of solidification, the front is a planar surface. As it strays from the copper surface, the solidification front becomes a parabolic surface, due to the limited insulation of the suspension from the air surrounding the polypropylene tube, almost invisible to X-ray. In order to limit the perturbation of the images in the radiography and tomography, a limited insulation was provided. Finite element analysis was used for estimating the shape of the solidification front, and correcting the systematic error. Figure 8 shows the shape of the front during three instants of the solidification with the temperature profile "*par1*." In order to minimize the error due to the shape of the solidification front, a reference position for the solidification front was estimated at 2/3 err from the upper limit, as shown in Fig. 8 on the left. Because of this correction, the error on the position of the front is 11 μm, due to the tomography resolution. When differentiating in order to obtain the velocity of the freezing front, this error approximately represents 1% of the measured velocity.

Figure 9 shows the plots of velocity of the freezing front as a function of time. The experimental results (test, solid line) are compared with the results by finite elements (FE, dashed line) and analytical model (ODE, meshed pattern line). The velocity was calculated by the position of the freezing front, considered as the projection of the front on the mold, and corrected

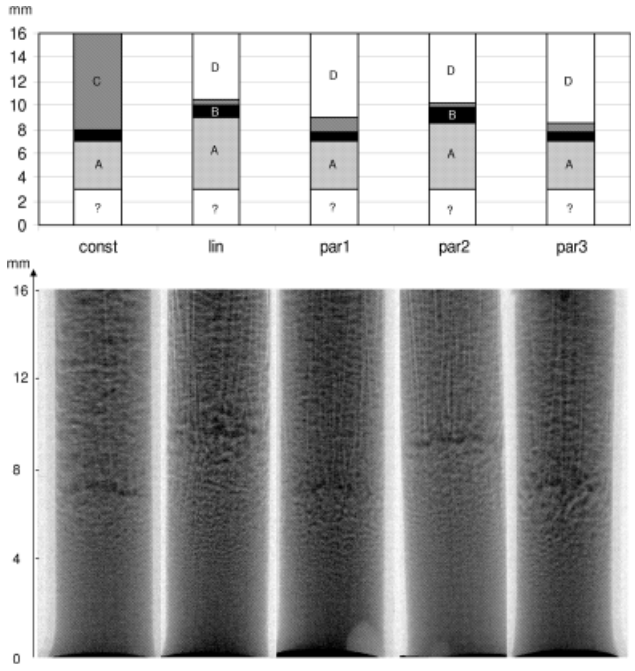

Fig. 6. The four morphological zones for the all the temperature profiles. The upper diagram shows the subdivision of each sample in the morphological zones. The lower diagram shows the results of the radiography at the end of the solidification process.

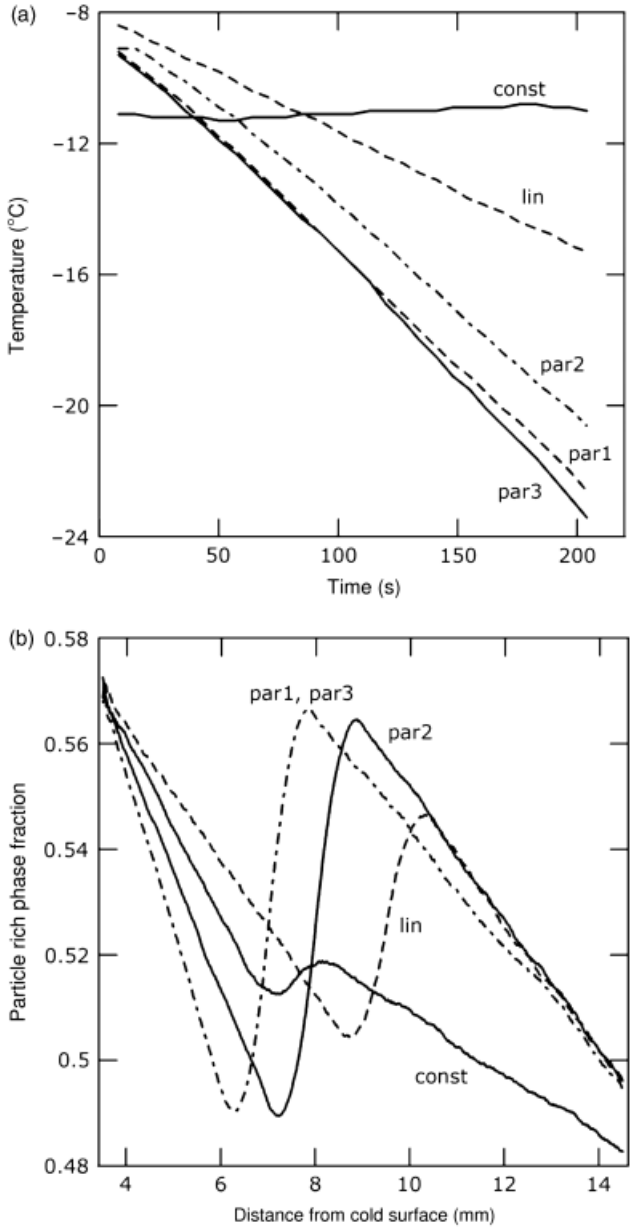

Fig. 7. The upper diagram shows the temperature profiles applied at the base of the colloidal suspension (a). The lower diagram shows the particle fraction as a function of the distance from the base of the suspension, plotted for all the temperature profiles (b).

according to the error estimation described at the beginning of the paragraph. The predictions by finite elements approximately follow the results by experimental tests, with a slight underestimation compared with the tests. The analytical model overestimates the velocity of the freezing front. A perfect fit of the analytical results with the tests was not expected. The parabolic profiles of temperature at the copper finger were used in order to minimize the decrease of the velocity of the freezing front as the distance between the copper finger and the front increases. This is useful to obtain as soon as possible the steady-state morphology of the crystals (zone D). According to Fig. 9, the velocity profiles "*par1*" and "*par3*" are the most efficient, shifting backward the transition zone and leaving more space for developing the zone D, and this is confirmed by the finite element analysis and by the analytical model. This behavior can be explained by the analytical model. For a Lewis number of 200–230 (Fig. 3), Brownian diffusion is quite high. The driving force for solidification is the undercooling at the base of the suspension. At slow solidification rates, the particles easily diffuse away from the

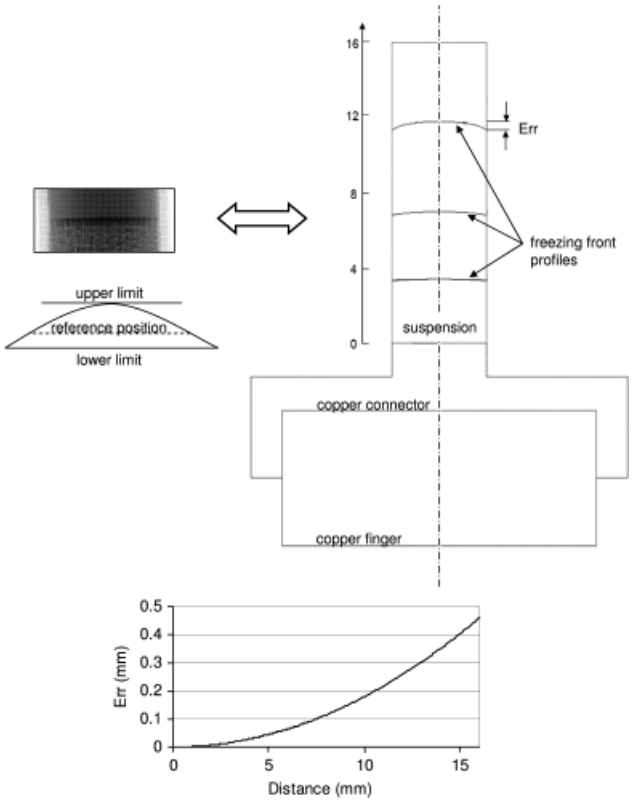

Fig. 8. The correction of the error due to the shape of the solidification front. The diagram on the right shows the prediction by finite elements of the shape of the solidification front in three instants of the process. The uncertainty generated by the shape of the freezing front presents an upper and a lower limit. The error, defined as the difference between the upper and the lower limit, is plotted in the bottom diagram.

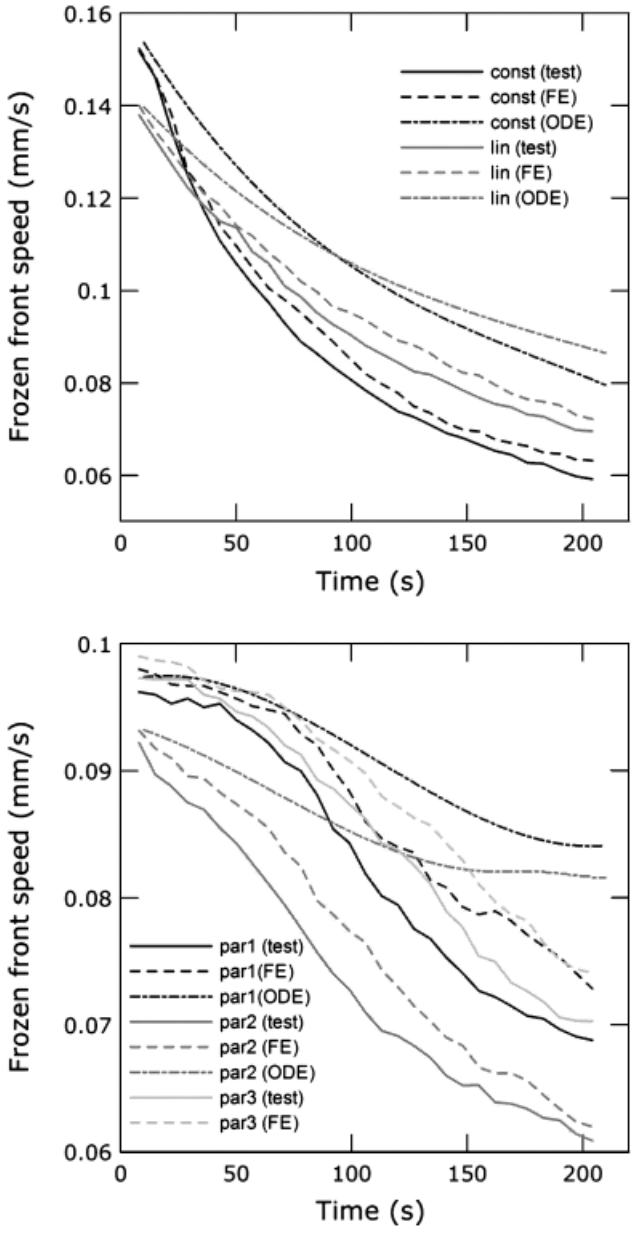

Fig. 9. The comparative diagrams of the velocity of the freezing front. The experimental results (test, solid line) are compared with the results by finite elements (FE, dashed line) and analytical model (ordinary differential equations (ODE), meshed pattern line). The upper diagram shows the velocities of the freezing front when a constant or linear temperature profile is applied at the base of the suspension (a). The lower diagram shows the velocities in the cases of the parabolic temperature profiles (b). The velocity was calculated by differentiating the position of the freezing front, considered as the projection of the front on the mold, and corrected according to the error estimation described by Fig. 8.

interface and the temperature of the suspension ahead of the interface is always warmer than the freezing temperature. At faster solidification rates, the concentration and concentration gradient increase at the interface. When the concentration gradient at the interface is steep enough that the gradient in the freezing temperature is larger than the temperature gradient (a minimum of the particle fraction in Fig. 7), the suspension ahead of the interface is below its freezing temperature (constitutionally supercooled). In analogy with binary alloys, constitutional supercooling is closely related to morphological instability, according to Davis.[26] By controlling the temperature at the base of the suspension it is possible to control the extension of the Z-crystals zone. A steep parabolic profile of the temperature maximizes the extension of the Z-crystals zone by a strong reduction of the transition zone (that also reduces the extension of the zone B). The lower parabolic temperature profile at the base of the suspension is associated with a shift of the transition zone toward the base of the suspension, leaving more space for the Z-crystals to develop.

IV. Conclusions

This paper investigates the dynamics of the solidification front in the ice templating of alumina colloidal suspension. The methods used include experimental tests, FEM, and analytical modeling. The comparison of the results complementary by the three approaches shows that the control of the morphology of packed alumina structures in the vertical direction can be achieved by choosing the profile of the temperature at the base of the suspension. The analytical model estimates the thermal properties of the colloidal suspension used in the FEM. Also the analytical model provides the estimation of the number of Lewis *Le* and the diffusion coefficient *D*, which resulted to be the most important parameters to predict the morphological behavior of colloidal suspension.[18,26] The analytical works presented in this paper allow estimating *Le* and *D* as a function of the medium properties, the particle radius, and the concentration of alumina. Future works should investigate the impact of the dispersant on the number of Lewis.

According to the experimental tests, to the finite element analysis and to the solution of the Stefan problem, a successful approach consists in applying a cooling rate approximately between 2 and 4°C/min; as the transition zone occurs, it is worth increasing the cooling rate following a parabolic profile. Because

the position of the transition zone is *a priori* unknown, it is convenient to apply a parabolic profile since the beginning of the process.

Appendix A: Details of the Analytical Model

The Stefan problem requires the estimation of the numbers of Stefan (St) and Lewis (Le). The two numbers are defined as follows:

$$St = \frac{L_f}{\rho C_p T},\ Le = \frac{\alpha}{D_0} \tag{A-1}$$

where L_f is the latent heat of fusion of water, ρ and C_p are, respectively, the density and the specific heat capacity of the suspension, α is the thermal diffusivity of the suspension $\left(\alpha \equiv \frac{k_T}{\rho C_p}\right)$, T is the absolute local temperature of the suspension, and D_0 is the Stokes–Einstein diffusivity, defined as follows:

$$D_0 = \frac{k_B T}{6\pi R\mu} \tag{A-2}$$

where k_B is the Boltzmann's constant, R the radius of the alumina particle, μ the dynamic viscosity of the carrying fluid. In order to calculate the numbers of Stefan and Lewis, the thermal properties of the suspension were estimated for the liquid and the solid phases.

The thermal conductivity was estimated by the equation of Jeffrey[14] used for modeling the thermal conductivity of the suspension (A-3):

$$\begin{aligned} k_{TS} &= k_{fluid}(1 + 3C_{vol}\beta + 3\Phi_{vol}^2\beta^2\gamma) \\ \gamma &= 1 + \frac{\beta}{4} + \frac{3\beta}{16}\frac{\alpha+2}{2\alpha+3}, \alpha = \frac{k_{ice}}{k_{fluid}}, \beta = \frac{\alpha-1}{\alpha+2} \end{aligned} \tag{A-3}$$

where $k_{ice,\ fluid}$ is the thermal conductivities of the medium (water) in the solid and in the liquid phase, and ϕ_{vol} the nominal volumetric concentration of the alumina particles $k_{ice} = 2.2(W \cdot (m \cdot K)^{-1}), k_{fluid} = 0.6(J \cdot (kg \cdot K)^{-1}), \Phi_{vol} = 0.32$.

The thermal conductivity of the suspension after freezing can be obtained by (A-3) and is equal to $k_{TS} = 0.9187(J \cdot (kg \cdot K)^{-1})$. The thermal conductivity of the suspension before freezing can be approximated by the thermal conductivity of the medium (liquid water)[12]: $k_{TL} = 0.6$ $(J \cdot (kg \cdot K)^{-1})$. For concentrations $C_{vol} < 0.5$, the specific heat capacity and the density of the suspension (C_p and ρ) can be estimated by the following relation:

$$C_p, \rho_{L,S} = (1 - \Phi_P)C_p, \rho_{water(L,S)} + (\Phi_P)C_p, \rho_{part} \tag{A-4}$$

where $\phi_p = 0.58$ is the packing fraction of particle in the suspension in the concentrated region between the ice crystals at ambient temperature and pressure. The Stokes–Einstein diffusivity has also been used by Peppin *et al.*[13] for writing the diffusion coefficient as a function of the local absolute temperature T and the local particle fraction ϕ

$$\begin{aligned} D(\Phi, T) &= D_0\hat{D}(\Phi), \\ \hat{D}(\Phi) &= (1 - \Phi)^6\frac{d(\Phi z)}{d\Phi} \end{aligned} \tag{A-5}$$

where z is the dimensionless compressibility factor which accounts for the effect of particle–particle interactions on the osmotic pressure $\Pi(\Phi)$, which can be written as

$$\Pi(\Phi) = \frac{\Phi}{v_p}k_B T z(\Phi) \tag{A-6}$$

The expression of the osmotic pressure as a function of the particle fraction is a fundamental result from statistical mechanics[27] which states that the osmotic pressure of a suspension of particles and the pressure of a perfect gas are the same functions of volume fraction if the particle–particle interaction potential is the same. Peppin *et al.*[13] propose the following estimation of the compressibility factor:

$$\begin{aligned} z(\Phi) &= \frac{1 + a_1\Phi + a_2\Phi^2 + a_3\Phi^3 + a_4\Phi^4}{1 - \Phi/\Phi_P}, \\ a_1 &= 4 - 1/\Phi_P, a_2 = 10 - 4/\Phi_P, \\ a_3 &= 18 - 10/\Phi_P, a_2 = 1.5/\Phi_P^5 - 18/\Phi_P \end{aligned} \tag{A-7}$$

Peppin *et al.*[13] obtained the freezing temperature by utilizing the conditions for local thermodynamic equilibrium between the liquid phase and the solid phase, assuming a planar interface and isotropic stress between the two phases, and the latent heat of fusion was approximately constant in the temperature range considered. From these assumptions, Peppin obtains the value of the freezing temperature $T_f(\Phi)$

$$\begin{aligned} T_f &= T_m(1 + mz\Phi)^{-1} \\ m &= \frac{k_B T_m}{v_p \rho_L L_f} \end{aligned} \tag{A-8}$$

with $T_m = 273$ K, the melting temperature of water.

Once the thermal properties of the suspension (k_T, C_p, and ρ), the diffusion coefficient D and the freezing temperature T_f have been estimated, the Stefan problem for unidirectional solidification of the suspension of hard-sphere colloids can be formulated. Figure 2 shows the quantities involved in the formulation of the Stefan problem as a function of ϕ. The Stefan problem is a system of two ODE and its solution represents the temperature field and the position $h(t)$ of the solidification front. Equation(A-9) shows the ODEs of the Stefan problem with the boundary conditions

$$\begin{aligned} \frac{\partial\Phi}{\partial t} &= \frac{\partial}{\partial x}D\frac{\partial\Phi}{\partial x} \\ B.C.\ \Phi &= \Phi_p(x = 0, t = 0) \\ \Phi\frac{\partial h}{\partial t} &= -D\frac{\partial\Phi}{\partial x}\ \ (x = t) \\ &\quad \text{and} \\ \frac{\partial T}{\partial t} &= \alpha\frac{\partial^2 T}{\partial x^2} \\ B.C.\ T &= T_b(t)(x = 0) \\ \rho L_f\frac{\partial h}{\partial t} &= k_T\left(\left.\frac{\partial T}{\partial x}\right|_{x=h^-} - \left.\frac{\partial T}{\partial x}\right|_{x=h^+}\right) \\ &\quad (x = h,\ T = T_f(\Phi))\ \text{Stefan condition} \end{aligned} \tag{A-9, Stefan problem}$$

The Stefan problem admits a similarity solution[16] with the variable

$$\begin{aligned} \eta &= \frac{x}{\sqrt{4D_0 t}}, \\ &\text{the interface position } h(t) = 2\lambda\sqrt{D_0 t}, \\ &\text{and the dimensionless temperature} \\ \theta &= \frac{T - T_\infty}{T_f - T_\infty} \end{aligned} \tag{A-10}$$

The formulation of the Stefan problem is

$$\begin{aligned}
&\frac{\partial \Phi}{\partial \eta} = -\frac{1}{2\eta}\frac{\partial}{\partial \eta} D(\Phi)\frac{\partial \Phi}{\partial \eta} \\
&\frac{\partial \theta}{\partial \eta} = -\frac{Le}{2\eta}\frac{\partial^2 \theta}{\partial \eta^2} \\
&\qquad B.C. \\
&\Phi = \Phi_p(\eta = 0) \\
&\theta = \theta_h(\eta), \Phi = \Phi_h(\eta), \Phi\lambda = \frac{D(\Phi)}{2}\frac{\partial \Phi}{\partial \eta}\bigg|_{\eta=\lambda} (\eta = \lambda) \\
&\text{with } \theta_h = \theta_m + \Gamma \frac{\Phi_h z}{1 + m\Phi_h z}\bigg|_h, \Gamma = \frac{mT_m}{T_\infty - T_f(\Phi_\infty)}\bigg|_{\Phi_\infty}
\end{aligned} \tag{A-11}$$

The problem was solved by using the MATLAB ODE suite, according to the methods illustrated by Shampine and Reichelt.[28] By substituting the results for φ in the Stephan condition ($\eta = \lambda$), it is possible to obtain the expression of λ for each boundary condition:

$$\lambda(t) = -\frac{Le}{2St}\left(\frac{\partial \theta}{\partial \eta}\bigg|_{\eta=\lambda-} - \frac{\partial \theta}{\partial \eta}\bigg|_{\eta=\lambda+}\right)(\eta = \lambda) \tag{A-12}$$

References

[1]W. A. Maxwell, R. S. Gurnick, and A. C. Francisco, "Preliminary Investigation of the Freeze-Casting Method for Forming Refractory Powders," *NACA Res. Memo*., **E53L21**, 1–19 (1954).

[2]K. Araki and J. W. Halloran, "Porous Ceramic Bodies with Interconnected Pore Channels by a Novel Freeze Casting Technique," *J. Am. Ceram. Soc*., **88**, 1108–14 (2005).

[3]K. Araki and J. W. Halloran, "New Freeze-Casting Technique for Ceramics with Sublimable Vehicles," *J. Am. Ceram. Soc*., **87**, 1859–63 (2004).

[4]U. Soltmann, H. Bottcher, D. Koch, and G. Grathwohl, "Freeze Gelation: A New Option for the Production of Biological Ceramic Composites (Biocers)," *Mater. Lett*., **57** [19] 2861–65 (2003).

[5]S. Deville, "Freeze-Casting of Porous Ceramics: A Review of Current Achievements and Issues," *Adv. Eng. Mater*., **10**, 155–69 (2008).

[6]T. Fukasawa, Z.-Y. Deng, M. Ando, T. Ohji, and S. Kanzaki, "Synthesis of Porous Silicon Nitride with Unidirectionally Aligned Channels Using Freeze-Drying Process," *J. Am. Ceram. Soc*., **85**, 2151–5 (2002).

[7]T. Fukasawa, M. Ando, T. Ohji, and S. Kanzaki, "Synthesis of Porous Ceramics with Complex Pore Structure by Freeze-Dry Processing," *J. Am. Ceram. Soc*., **84**, 230–2 (2001).

[8]S. Deville, E. Saiz, and A. P. Tomsia, "Ice-Templated Porous Alumina Structures," *Acta Mater*., **55**, 1965–74 (2007).

[9]S. Deville, E. Maire, A. Lasalle, A. Bogner, C. Gauthier, J. Leloup, and C. Guizard, "In Situ X-Ray Radiography and Tomography Observations of the Solidification of Aqueous Alumina Particle Suspensions—Part I: Initial Instants," *J. Am. Ceram. Soc*., **92**, 2489–96 (2009).

[10]E. Maire, A. Fazekas, L. Salvo, R. Dendievel, S. Youssef, P. Cloetens, and J. M. Letang, "X-Ray Tomography Applied to the Characterization of Cellular Materials. Related Finite Element Modeling Problems," *Compos. Sci. Technol*., **63**, 2431–43 (2003).

[11]J.-Y. Buffiere, E. Maire, J. Adrien, J.-P. Masse, and E. Boller, "In Situ Experiments with X Ray Tomography: An Attractive Tool for Experimental Mechanics," *Exp. Mech*., **50** [3] 289–305 (2010).

[12]P. W. Egolf and H. Manz, "Theory and Modelling of Phase Change Materials with and Without Mushy Regions," *Int. J. Heat Mass Transfer*, **37** [18] 2917–24 (1994).

[13]S. S. L. Peppin, J. A. W. Elliott, and M. G. Worster, "Solidification of Colloidal Suspensions," *J. Fluid Mech*., **554**, 147–66 (2006).

[14]D. J. Jeffrey, "Conduction Through a Random Suspension of Spheres," *Proc. R. Soc. London*, **335**, 355–67 (1973).

[15]A. S. Barr and E. Luijten, "Structural Properties of Materials Created Through Freeze Casting," *Acta Mater*., **58** [2] 709–15 (2010).

[16]L. I. Rubinstein, "The Stefan Problem," *Am. Math. Soc*., **27** (1971). (Translated from Russian).

[17]E. Thiele, "Equation of State for Hard Spheres," *J. Chem. Phys*., **39**, 474–9 (1963).

[18]D. A. McQuarrie, *Statistical Mechanics*. Harper & Row, New York, 1986.

[19]W. B. Russel, D. A. Saville, and W. R. Schowalter, *Colloidal Dispersions*. Cambridge University Press, Cambridge, 1989.

[20]F. H. Ree and W. G. Hoover, "Fifth and Sixth Virial Coefficients for Hard Spheres and Hard Disks," *J. Chem. Phys*., **40**, 939–50 (1964).

[21]L. V. Woodcock, "Glass Transition in the Hard-Sphere Model and Kauzmann's Paradox," *Ann. New York Acad. Sci*., **371**, 274–98 (1981).

[22]N. F. Carnahan and K. E. Starling, "Equation of State for Nonattracting Rigid Spheres," *J. Chem. Phys*., **51**, 635–6 (1969).

[23]K. E. Davis, W. B. Russel, and W. J. Glantschnig, "Disorder-to-Order Transition in Settling Suspensions of Colloidal Silica: X-Ray Measurements," *Science*, **245**, 507–10 (1989).

[24]M. G. Worster, "Solidification of Fluids"; pp. 393–446, *Perspectives in Fluid Dynamics*, Edited by G. K. Batchelor, H. K. Moatt & M. G. Worster. Cambridge University Press, Cambridge, 2000.

[25]S. R. Coriell and R. F. Sekerka, "Oscillatory Morphological Instabilities Due to Non-Equilibrium Segregation," *J. Cryst. Growth*, **61**, 499–508 (1983).

[26]S. H. Davis, *Theory of Solidification*. Cambridge University Press, Cambridge, 2001.

[27]W. G. McMillan and J. E. Mayer, "Statistical Mechanics of Multicomponent Systems," *J. Chem. Phys*., **13**, 276–305 (1945).

[28]L. F. Shampine and M. W. Reichelt, "The MATLAB ODE Suite," *SIAM J. Sci. Comput*., **18**, 1–22 (1997). □